ISOTHERMAL SOLIDIFICATION IN A BINARY ALLOY MELT

Principal Investigator : V.Laxmanan, Department of Metallurgy & Materials Science, Case Western Reserve University, Cleveland, Ohio 44106. Concurrently, Visiting Scientist, NASA Lewis Research Center, Mail Stop 105-1, Cleveland, Ohio 44135.

ABSTRACT

A space shuttle experiment employing the General Purpose (Rocket) Furnace (GPF) in its isothermal mode of operation is manifested on MSL-3, circa 1989. The central aim of this experiment (first in a series of proposed experiments) is to investigate the effect of reduced gravity gravity levels on the segregation behavior in a slowly, and isothermally, cooled sample (cooling rate 0.003 K/sec, thermal gradients < 0.05 K/mm, the top is slightly hotter than the bottom) of a binary Pb-15 wt% Sn alloy. This experiment would thus be able to simulate, in a small laboratory sample, about 20 mm dia 60 mm high and weighing about 150 grams, some aspects of the segregation phenomena occurring in large industrial ingots. Ground-based experiments conducted in the single-cavity simulator of the GPF, located at the Marshall Space Flight Center (MSFC), in support of the microgravity experiment are described in detail. The results of the MSFC experiments are compared with other related experiments conducted at Case Western Reserve University (CWRU), wherein the isothermal constraints were relaxed.

The isothermally processed samples indicate a small and gradual increase in fraction eutectic , and a corresponding increase in tin content, from the bottom to the top of the ingot. At a given height from the ingot bottom, we also observe a radial variation of eutectic fraction, or tin content. The radial variations are minimal near the ingot bottom, but there are large radial variations in the top half. The microgravity experiment would most likely indicate a smaller variation in fraction eutectic from the bottom to the top. Also, the large radial variations near the top would be much less pronounced, if not totally absent. In the CWRU experiments, we have been able to simulate more severe segregation, including segregation defects known as freckles. Follow up experiments employing the GPF without the isothermal constraints, or other suitably modified space shuttle hardware are suggested.

Introduction

When a molten alloy is allowed to freeze a number of important physical factors come into play which together contribute to the formation of a solid phase of non-uniform composition. First, the density of the solid and liquid phases are different, i.e., the fractional density change

$$\beta = (\rho_s - \rho_L) / {}_s > 0,$$

resulting either in liquid flow towards the freezing regions to feed shrinkage ($\beta > 0$) or flow away from the solid-liquid interface if $\beta < 0$. Here ρ_s is the density of the solid and ρ_L the density of the liquid. Second, the latent of fusion liberated during solidification must be transported away from the solid-liquid interface, resulting in temperature gradients in the liquid and solid phases. Third, the various alloying elements redistribute themselves differently between the liquid and solid phases, i.e., the partition ration $k > 1$ or $k < 1$. The remanent liquid is thus either enriched ($k < 1$) or depleted ($k > 1$) in alloying elements, resulting in a continuously changing liquid composition and hence a continuously changing solid composition. There is little that can be done to alter these three factors, which are dictated solely by fundamental physical and chemical laws governing the atomic or molecular arrangements in the solid and liquid states. The final solid formed is thus necessarily inhomogeneous in composition.

In terrestrial solidification processes, the inevitable segregation resulting from the fact that $k \neq 1$, and/or $\beta \neq 0$, is further aggravated by the complicating effects of gravity-driven fluid flow. Temperature and concentration gradients within the liquid phase give rise to density gradients, which in turn leads to fluid motion within both the fully liquid and partially frozen regions of a freezing ingot. Also, in a gravity field, density differences between the solid and liquid phases can result in settling or floating of detached solid particles or dendrites, and hence segregation, due to this effect. Thus, gravity-driven fluid flow effects can lead to (large) compositional changes, occurring over distances of the order of the dimensions of the ingot. We refer to this as macro-segregation. In the absence of any significant gravitational fluid flow effects, compositional changes would be confined to distances on the order of the local primary or secondary dendrite arm spacings in a freezing ingot. We refer to this as micro-segregation. A more quantitative definition of macro- and microsegregation is given later.

It is now generally accepted [1-5] that gravity-driven fluid flow is the underlying cause for the severe segregation pattern often observed in many industrial solidification processes ("freckles" in superalloys, U, Nb base alloys and other specialty alloys, "A" and "V" segregates in steels, etc). Non-uniformity of composition reflects itself in an undesirable variation in mechanical, chemical, electrical, magnetic or other physical properties of the alloy and thus leads to an inferior performance during service. A great deal of experimental and theoretical effort has been expended over the years to understand the basic mechanisms responsible for the observed segregation behavior, and a number of control strategies have been proposed to minimize segregation defects. There is, however, much that remains to be learned from a fundamental standpoint.
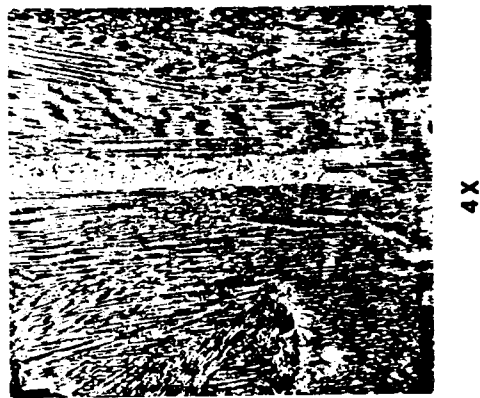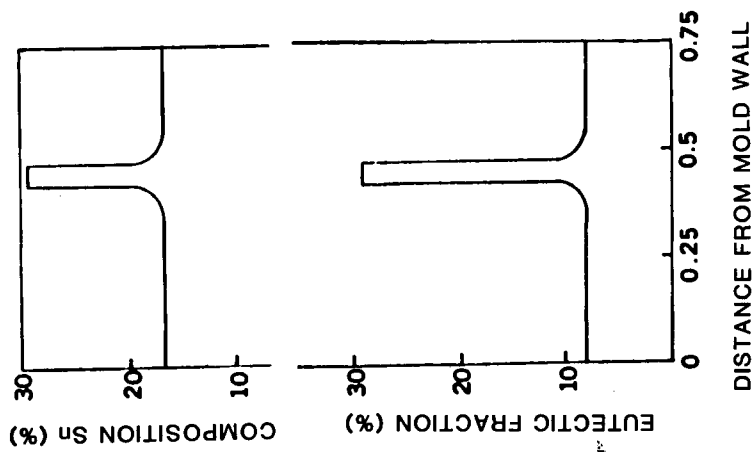
Fig. 1 : Columnar freckle in one of the CWRU experiments; Table 2, experiment
no. 4. The tin enriched region is slightly off-center with respect to
the ingot axis and extended approximately to the mid-height of the
ingot from the top.

The basic mechanisms leading to severe segregation defects such as "freckles"*, Figure 1, during alloy solidification are also quite similar to the mechanisms believed to be responsible for other natural processes such as atmospheric currents, and, thermo-haline or thermo-solutal convection responsible for ocean currents. In the presence of severe salinity gradients, thermosolutal convective effects can lead to the formation of "salt fingers" in oceans; the oceanographers analog of "freckles."[6] Thus, a fundamental understanding of segregation phenomena during alloy solidification has wider applications.

Experimental Approach: Justification for Microgravity

The principal objective of the experiments to be described here is to investigate the effect of reduced gravity levels on macro- and microsegregation in a slowly cooled sample of a model binary Pb-15 wt% Sn alloy. The reduced gravity experiment will be performed aboard the space shuttle. One currently approved microgravity experiment is manifested for flight on the MSL-3, circa 1989, and will employ the General Purpose (Rocket) Furnace (GPF) in its isothermal** mode of operation. A series of three other space shuttle experiments, also employing the GPF, has also been proposed [7]. These are aimed at investigating segregation behavior without the isothermal constraints imposed in the first experiment. Experiments of this type may, however, be satisfactorily performed in other experimental apparati, such as the ADSF or AADSF** with stationary sample of suitable aspect ratio, or even the IDGA.**

A number of ground-based (1-g) experiments have been carried out in the interim as a precursor to the microgravity experiments. The main purpose of this paper is to describe some of the important ground-based results obtained to date. The 1-g experiments may be divided into two categories. The first set involves tests conducted at the Marshall Space Flight Center (hereafter MSFC tests). These tests employed the single cavity simulator of the GPF. The MSFC tests were all aimed at:

i) Ensuring complete reproducibility, in earth-based studies, of the thermal conditions to be employed in the microgravity experiment. Thus, these tests were mainly concerned with achieving nearly isothermal conditions, to reflect the constraints imposed for the first space shuttle experiment. This has been accomplished successfully in many tests (12 to date), Table 1. A typical cooling rate in the MSFC test was 0.003 K/sec. Axial thermal gradients in the samples were often less than 0.05 K/mm. The GPF will be programmed to achieve identical thermal conditions in the space shuttle experiment.

ii) A detailed characterization of the thermal conditions within the solidifying sample using the maximum of six thermocouples which could

---

* A "freckle" is a long column or extended region of solute enriched or solute depleted material. The term solute is used here to denote the minor species in a binary or multi-component alloy.

** This constraint was imposed by MSFC back in April 1984 when this experiment was first proposed. The "isothermal" experiment was originally scheduled to fly on the D-1 mission, then planned for October/November 1985. IDGA: Isothermal Dendrite Growth Apparatus. AADSF: Advanced Automatic Directional Solidification Furnace.

HEAT NUMBER	CHEMICAL COMPOSITION		SOLIDIFICATION TIME, min	COOLING RATE c/min	TEMPERATURE GRADIENT G, c/cm	LIQUIDUS ISOTHERM VELOCITY R_t, cm/min	FRECKLES
	Pb%	Sn%					
1	85.1	14.9	65	3.23	1.54	2.0830	NO
2	85.1	14.9	150	1.21	16.85	0.0718	NO
3	84.7	15.3	230	0.98	24.70	0.0397	NO
4	84.8	15.2	350	0.55	22.32	0.0246	YES
5	86.0	14.0	520	0.425	34.25	0.0124	YES
6	85.0	15.0	300	0.713	21.10	0.0338	?
7	15.0	85.0	59	2.32	27.56	0.0842	NO
8	15.7	84.3	135	0.89	19.49	0.0354	NO
9	15.6	84.4	170	0.69	16.14	0.0551	NO

CD-86-20012

Table 1 : Summary of important solidification parameters in the samples processed at CWRU.

SAMPLE	COOLING RATE, K/SEC	AVERAGE TEMPERATURE GRADIENT, K/MM	QUENCH TEMPERATURE, ^{0}C	COMMENTS
LERC001	0.0030	0.051	164.5	MULTIPLE HEATS
LERC002	0.0030	0.011	169.2	PRELIMINARY CARTRIDGE DESIGN
LERC003	0.0029	0.092	269.0	
LERC004	0.0031	0.078	259.5	
LERC005	0.0030	0.070	164.0	
LERC006	0.0033	0.025	164.5	FINAL PLUNGER DESIGN
LERC008	0.0086	0.028	281.0	
LERC010	0.0036	0.097	285.0	TWO HEATS

*TEMPERATURE GRADIENT IN SAMPLE WAS REQUIRED TO BE LESS THAN 0.1 K/MM. TEMPERATURE GRADIENT DECREASES AS MORE AND MORE SOLID FORMS.

CD-87-24853

Table 2 : Summary of processing conditions in the single-cavity simulator of the GPF located at MSFC.

be accommodated with the single-cavity GPF simulator. Only two thermocouples are permitted in the microgravity experiment.

iii) Tracking the evolution of segregation in the sample under 1-g conditions by interrupting the solidification and rapidly quenching the partially frozen alloy, thus preserving the high temperature structure. The samples were quenched from various temperatures within the liquid-solid range prior to complete solidification of the alloy.

The MSFC tests thus represent the most critical and extensive 1-g data base for the microgravity experiment.

The second set of experiments, summarized in Table 2, are the 1-g tests conducted at Case Western Reserve University (hereafter CWRU tests), in an apparatus which was built to mimic the essential thermal characteristics of the GPF. These tests were conducted over a much wider range of thermal gradients and cooling rates. Cooling rates were varied between 30 K/sec and 210 K/sec whereas thermal gradients varied between 0.15 K/mm to 3.5 K/mm. These thermal conditions are well within the capabilities of the GPF, and represent experimental conditions that could be employed in potential future space shuttle experiments, or looking even further, in materials processing experiments in the space station.

Thus, in these ground-based experiments, we have been able to simulate some aspects of the segregation phenomena occurring in large industrial ingots in a relatively small laboratory sample - about 20 mm dia., 60 mm high, and weighing about 150 gram - under carefully controlled conditions. The MSFC tests simulate the solidification behavior in the interior of large, statically cast, industrial ingots wherein solidification occurs over long periods of time, often 2 to 3 days, with negligibly small thermal gradients and cooling rates. Typical solidification time in the MSFC test was about 640 minutes, i.e., the alloy was partially solid for nearly 11 hours. An important outcome of the first microgravity experiment would be a clear demonstration of the relative importance of fluid flow due to shrinkage and gravitational effects. If shrinkage flows are predominant, or at least as important as gravitational effects, a potentially useful strategy for controlling macrosegregation on earth would be to manipulate the alloy composition to achieve negligibly small density differences between the liquid and solid phases ($\beta \rightarrow 0$).

The CWRU tests, on the other hand, simulate the thermal conditions attained in a number of other industrial solidification processes - continuous casting, ESR or VAR ingots, for example. In these tests we have been able to produce more severe segregation, including "freckles", illustrated earlier in Figure 1. Again, the microgravity experiment would help elucidate the fundamental role of gravity in triggering these severe segregation defects. For example, in experiments wherein the thermal (and hence the density) gradient is somewhat steeper, freckles were observed, whereas in others with a smaller thermal gradient only a pronounced compositional change from the top to bottom is observed: see figure 16, later in this paper which summarizes the compositional data for experiments in Table 2. Experiments No. 4, 5, and 6 are particularly noteworthy.

432

Unique Features of the GPF-type Experiments: Comparison with DS Experiments

In the binary Pb-15 wt% Sn alloy, solidification begins at the liquidus temperature ($T_L \sim 290°C$).Liquid becomes enriched in Sn as solidification proceeds and solidification ends at the eutectic temperature ($T_E = 183°C$) when a fraction f_E of the original liquid freezes as a two-phase solid. Thus, solidification occurs over a very wide range of temperatures in this alloy, from approximately $290°C$ to $183°C$, or over an interval of about $100°C$. Since the maximum ingot dimension, the height, is only about 50 to 60 mm in the GPF experiments, axial thermal gradients considerably less than 2 K/mm will result in the formation of a two-phase region of part liquid and part solid, the so-called mushy zone, throughout the entire ingot.

We define a fully developed mushy zone (FDMZ) as a mushy zone bounded at the top by the liquidus isotherm, T_L, and at the bottom by the eutectic isotherm, T_E. A partially developed mushy zone (PDMZ), on the other hand, is one that may be bounded at the top by an isotherm $T < T_L$ and at the bottom by an isotherm $T > T_E$. The mushy zone is almost always completely developed in directional solidification (DS) experiments, wherein the velocity of the tip isotherm, R_t, is exactly equal to the velocity of the eutectic isotherm, R_E, both being exactly equal to the withdrawal speed of the sample, V, Figure 2. In principle, the tip temperature T_t in a DS experiment is always less than the liquidus temperature T_L. The dendrite tip undercooling

$$\Delta T = T_L - T_t$$

is a function of the growth

$$R (= R_t = R_E = V),$$

and the externally imposed thermal gradient G_l, but is negligibly small compared to the freezing range of the alloy* under most of the usual conditions of dendritic growth in alloys [8-10]. Also, the mushy zone thickness, M, remains constant in a typical DS experiment once steady-state conditions have been achieved.

In the GPF-type experiments on the other hand, the mushy zone thickness, M, is never constant, but changes slowly with time, depending on the thermal gradient and the cooling rate. These experiments are

---

* The equilibrium freezing range $\Delta T_0 = T_L - T_S$ is often used in the theory of dendritic solidification in alloys as the reference temperature for non-dimensionlization [9-12]. Thus, $\Delta T/\Delta T_0 \ll 1$ under the usual conditions of dendritic growth, typically only about 0.001 or less. The quantity $T_L - T_E$ is the non-equilibrium freezing range.

Non-equilibrium conditions prevail during most common experimental conditions because of relatively small rates of diffusion in the solid phase compared to the liquid [13]. We assume compositional equilibrium is achieved only "locally" at the solid-liquid interface.
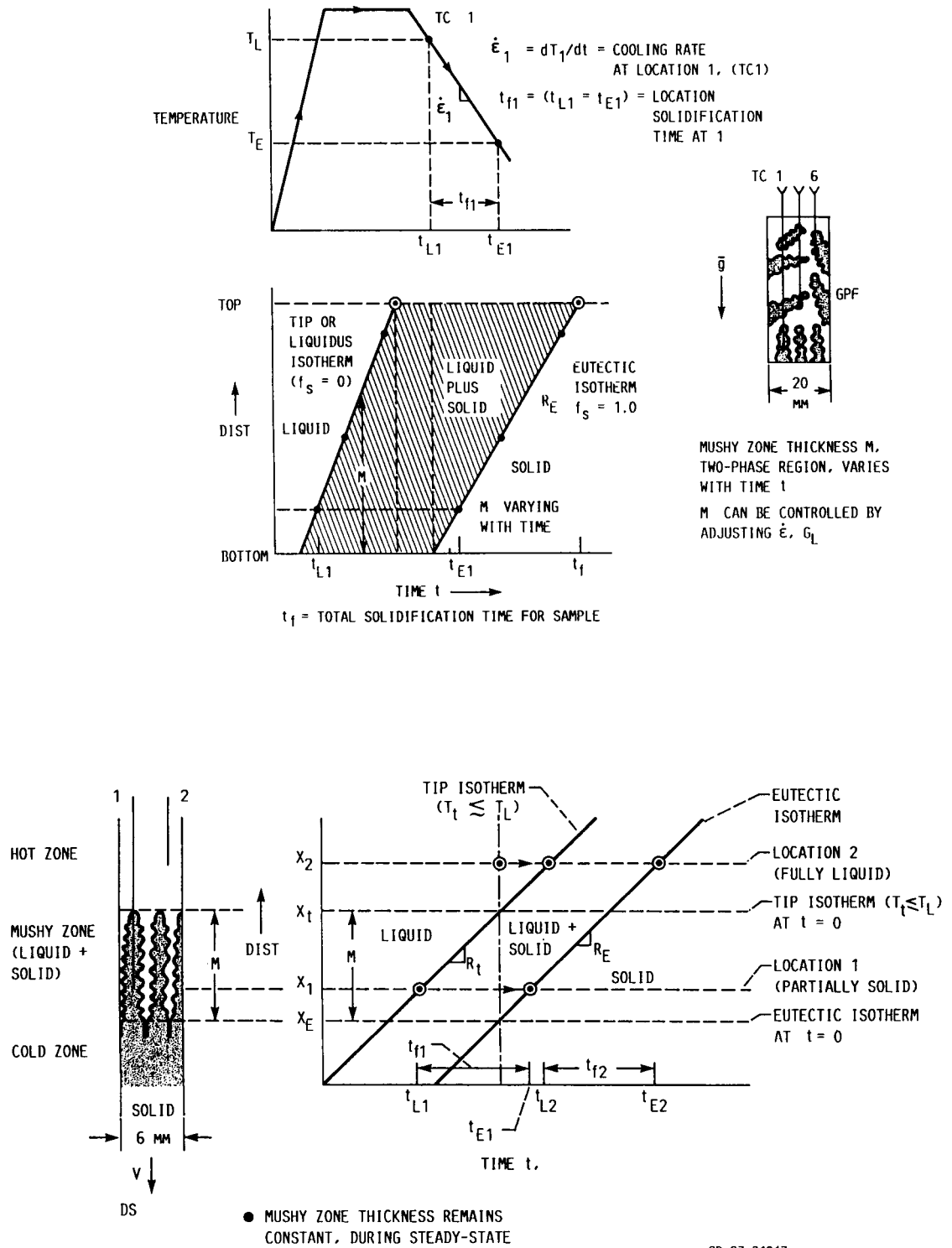
Fig. 2 : Comparison of mushy zone character in GPF-type experiment and directional solidification (DS) experiments.
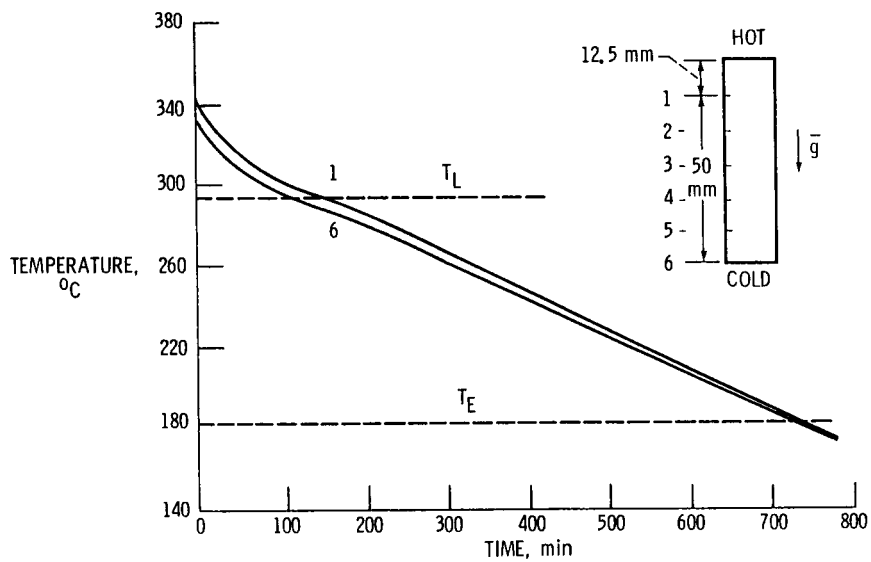
434

Fig. 3 : Typical temperature-time plot for slowly cooled sample in single-cavity GPF simulator; LeRC 002, Table 1.

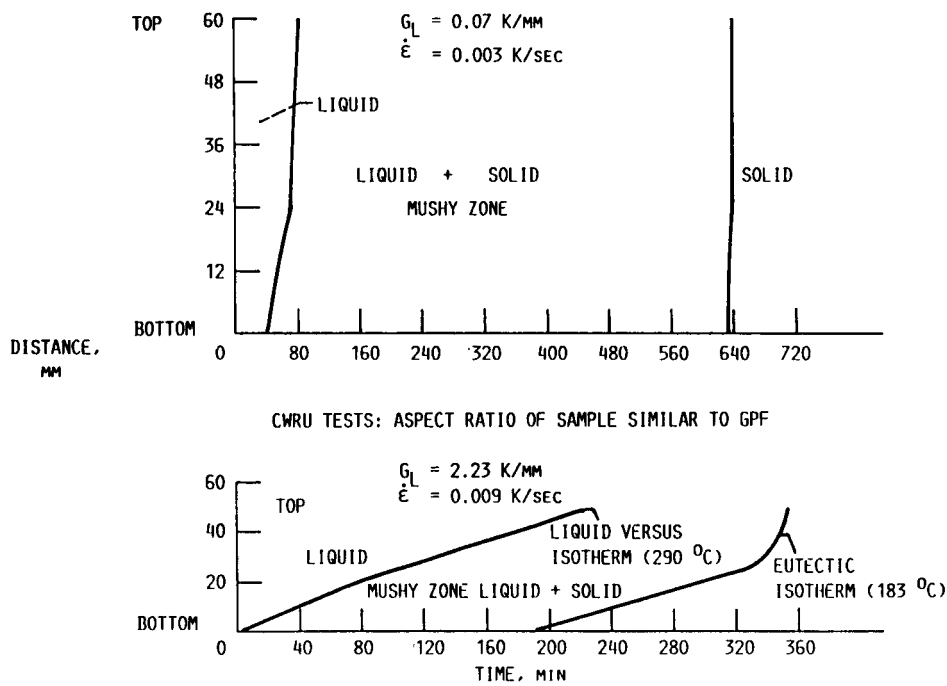CWRU TESTS: ASPECT RATIO OF SAMPLE SIMILAR TO GPF

Fig. 4 : Comparison of evolution of mushy zone (two-phase, liquid plus solid, region) in MSFC and CWRU experiments.

435

therefore uniquely suited to investigate the influence of gravity-driven fluid-flow effects on macro- and microsegregation during dendritic solidification. Moreover, both FDMZ's and PDMZ's can be created, with various bounding temperatures at the top and the bottom, see also Figure 5. The DS experiments do not allow such a flexibility.

Figure 3 plots the experimentally determined temperature-time profile at various locations in one of the MSFC tests. Figure 4 re-plots the same information differently. Here we imagine tracking the position of a given isotherm, say the eutectic or liquidus isotherm, in the sample as a function of time. Note that the ingot is partially solid i.e., mushy, (the dendritic network of solid has no particular directionality because of the nearly isothermal conditions prevailing, see microstructure of a partially quenched sample in Figure 11a)with a fully liquid zone above the mushy zone in the early stages of the experiment. The thickness of the mushy zone increases gradually with time, during the first 90 minutes or so, until the entire sample becomes liquid plus solid. This sequence of events is shown schematically in Figure 5. The sample remains part liquid plus solid during the greater part of the experiment, with the temperature decreasing slowly with time, and is abruptly frozen when the eutectic isotherm sweeps through the ingot. In the calculations in Figure 4, we assume that the liquidus isotherm of the original alloy demarcates the fully liquid region from the liquid plus solid region, i.e., we have implicity assumed that the bulk liquid composition remains unchanged and is always equal to the initial alloy composition of C_o = 15 wt% Sn.
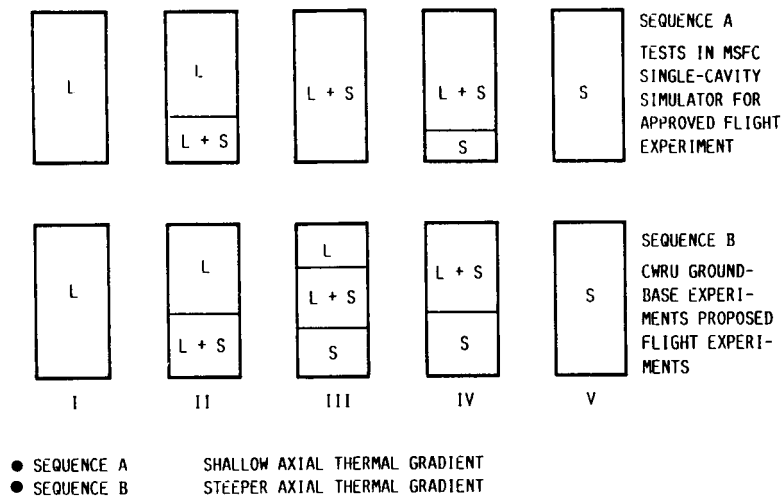
This is a questionable assumption, particularly because of the compositional changes occurring in the interdendritic liquid due to enrichment of Sn during the course of the experiment, and the attendant change in the bulk liquid if there is significant fluid motion. The spatial and temporal variation of the liquid composition is, however, unknown apriori without further detailed calculations and the above approximation is still a useful one to delineate the various phase regions.

A similar solidification sequence was observed in some of the CWRU tests, those with thermal gradients much less than 2 K/mm, the significance of which has been discussed earlier. Some of the CWRU tests, however, yielded a slightly different sequence because of the steeper thermal gradients employed. Figures 4b and 6 illustrate, for example, the thermal conditions which lead to the "freckle" noted in Figure 1. In this case, the mushy zone never penetrates the sample completely. A completely solid layer is formed at an early stage in the experiment. However, density gradients in this case are much greater in the corresponding MSFC tests. Figures 4 through 6 compares the solidification sequence in the MSFC and CWRU tests.

In summary, the GPF-type experiments of the type being planned for the proposed and approved space shuttle experiments offer a number of unique and innovative opportunities to critically examine the role of gravity-driven fluid flow effects.

Characterization of Macro- and Microsegregation

Consider a small volume element within a freezing alloy, Figure 7. The volume element is fixed in space and the dimensions of the element are supposed to be appropriate to the size scale of the dendrites growing in the melt and the local dendrite arm spacings. At time t < 0 the element is fully liquid. The temperature $T > T_L$ and the liquid composition within

SEQUENCE A

TESTS IN MSFC SINGLE-CAVITY SIMULATOR FOR APPROVED FLIGHT EXPERIMENT

SEQUENCE B

CWRU GROUND-BASE EXPERI-MENTS PROPOSED FLIGHT EXPERI-MENTS

I   II   III   IV   V

● SEQUENCE A   SHALLOW AXIAL THERMAL GRADIENT
● SEQUENCE B   STEEPER AXIAL THERMAL GRADIENT

CD-87-24846

Fig. 5 : Schematic illustration of sequence of solidification in GPF-type experiments. Fully developed mushy zone (FDMZ) is seen in sequence B, stage III. The mushy zone is partially developed in all other stages.
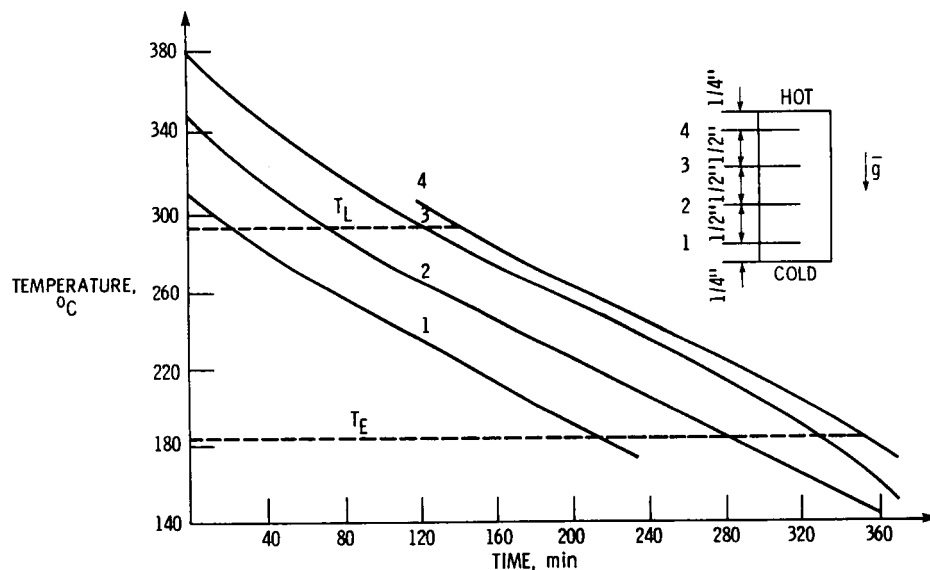
CD-86-20004

Fig. 6 : Temperature-time plot for slowly cooled sample in one of the CWRU experiments leading to the freckle illustrated in fig. 1. The axial thermal gradient is steeper than in the MSFC tests.
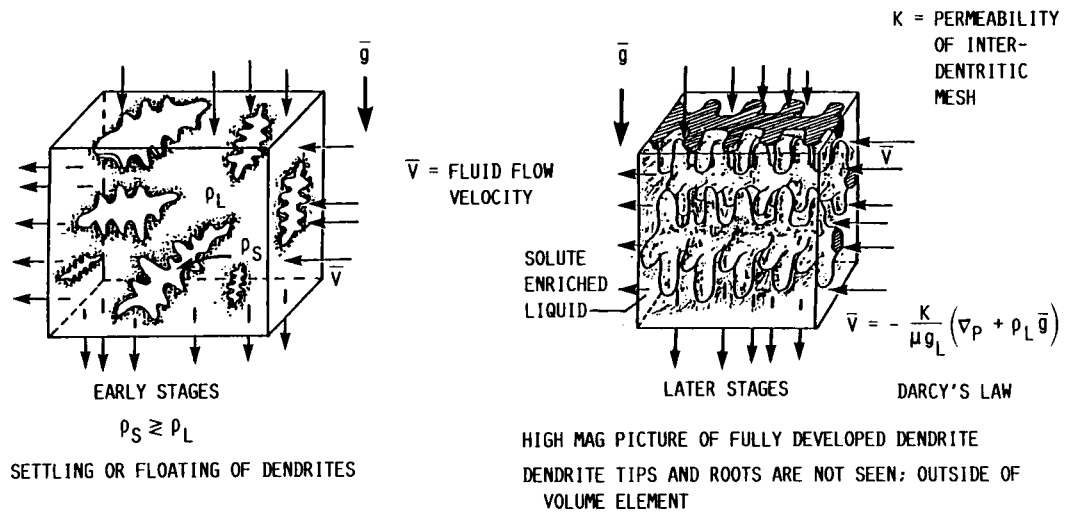
K = PERMEABILITY OF INTER-DENTRITIC MESH

$\bar{V}$ = FLUID FLOW VELOCITY

SOLUTE ENRICHED LIQUID

$$\bar{V} = - \frac{K}{\mu g_L}\left(\nabla_P + \rho_L \bar{g}\right)$$

EARLY STAGES

$\rho_S \gtrsim \rho_L$

SETTLING OR FLOATING OF DENDRITES

LATER STAGES   DARCY'S LAW

HIGH MAG PICTURE OF FULLY DEVELOPED DENDRITE

DENDRITE TIPS AND ROOTS ARE NOT SEEN; OUTSIDE OF VOLUME ELEMENT

Fig. 7 : Schematic illustration of small volume element undergoing solidification in an ingot.

- RELATIVELY LOW MAG PICTURE, ENTIRE DENDRITE SEEN
- LIQUID COMPOSITION INCREASING FROM TIPS TO ROOTS

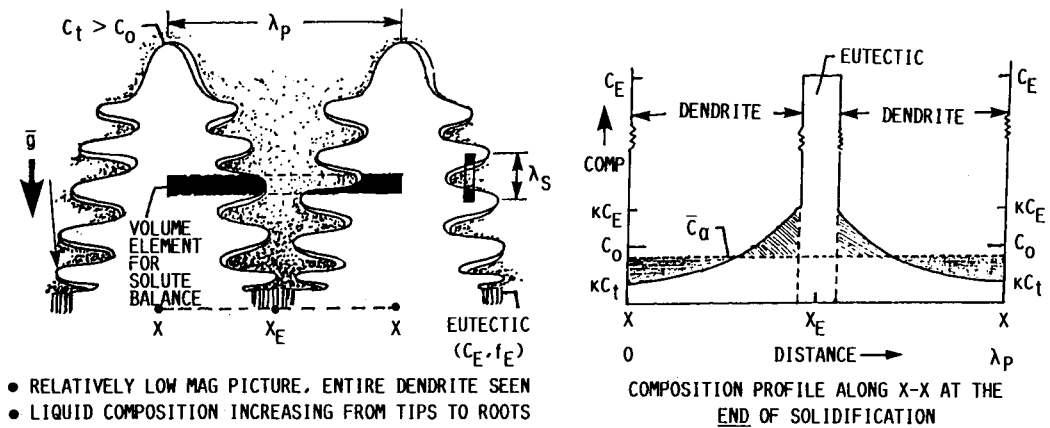COMPOSITION PROFILE ALONG X-X AT THE END OF SOLIDIFICATION

Fig. 8 : Microsegregation, i.e. compositional change, between the centerline of two individual dendrites.

438

the element is <u>assumed</u> to be uniform and equal to C_0. At t = 0 the temperature T has dropped to T_t and the dendritic array begins to sweep through the element. The first solid (dendrite tip) to form has a composition kC_t. Here T_t is the dendrite tip temperature and C_t is the liquid composition in equilibrium with the tips: $T_s < T_t < T_L$ and $C_0 < C_t < C_0/k$. The exact values of C_t and T_t depend on the dendrite tip growth rate R_t, the thermal gradient G_L in the liquid and the alloy composition [9-12]. As solidification proceeds fraction liquid within the element decreases and correspondingly the liquid composition increases (k < 1). Let C_L be the liquid composition within the element at time t when the liquid fraction remaining in the element is f_L. This is the situation depicted in Figure 7.

When the liquid composition within the element has increased to C_E, the eutectic composition, two-phase or eutectic solidification begins. Let $\bar{C}_\alpha$ denote the average composition of the dendritic solid within the element at this time, Figure 8, and let f_E denote the fraction of liquid remaining in the element just prior to the beginning of eutectic solidification. The volume element is completely frozen when the fraction liquid f_E freezes at the eutectic temperature, T_E.

The <u>average</u> composition of the dendrite, $\bar{C}_\alpha$, will be some unknown value between kC_t and kC_E, but must obviously be less than C_0, Figure 8. Let $\bar{C}_{\alpha\beta}$ denote the <u>average</u> composition of the two-phase or eutectic solid formed within the element, and, $\bar{C}_s$ the <u>average</u> composition of the finally solidified alloy, i.e., the average composition of the dendrite plus average composition of the two-phase solid:

$$\bar{C}_s = \bar{C}_\alpha \, f_\alpha + \bar{C}_{\alpha\beta} \, f_E \tag{1}$$

where $f_\alpha = 1 - f_E$. $\bar{C}_{\alpha\beta}$ depends on the growth rate of the eutectic front, R_E, and the thermal gradient. $\bar{C}_{\alpha\beta} = C_E$ only in the ideal case when the liquid is isothermal [14], i.e., when G_L/R_E is very small. $\bar{C}_{\alpha\beta} \to C_0$ for high values of G_L/R_E. The task at hand is now to calculate theoretically the values of $\bar{C}_\alpha$. $\bar{C}_{\alpha\beta}$ and f_α or f_E in Equation (1) above. A mathematically rigorous calculation, which also allows for fluid-flow effects, is admittedly very difficult to perform. A simple model, based on the work of Flemings, Hunt, and co-workers has recently been proposed by the author [15]. This is discussed later. Equation 1 may however be used to define quantitatively the basic notions of macro- and microsegregation.

In general, the average composition of the final solid formed within the volume element of Figure 7 may be greater than, equal to or less than the initial alloy composition C_0. If, perchance, $\bar{C}_s$ is exactly equal to C_0, we say that there is NO macrosegregation within this element. If the same situation exists within every single random volume element in the

casting or ingot* it is easy to visualize that there will be no "macroscale" variations in the average composition of the solid as we sample various portions of the ingot. The entire ingot will appear to be homogeneous in composition.

We may verify this for example by measuring the chemical composition by atomic absorption spectrometry, X-ray analysis, or wet chemistry tests, by taking small random drillings from various locations. Such chemical measurements are reported later. Or we may measure composition variations non-destructively by traversing a rather coarse or diffuse electron beam across various regions. The fraction eutectic f_E may also be used as a measure of the various in the average composition of the final solid. This offers another convenient non-destructive method of quantifying macrosegregation in the sample. A comparison of the results obtained from these various techniques is presented in Figure 9.

Note that even if $\bar{C}_s = C_0$, there are still compositional variations but these are strictly on a "microscopic" scale - the scale of the dendrite arm spacings. This is microsegregation, Figure 8. These microscopic variations can be detected by traversing small regions of the sample with a finely focused electron beam (microprobe analysis). Ideally we should be able to show that the average composition between any two dendrites or a group of dendrites is exactly equal to C_0, IF there is NO macrosegregation. Unfortunately, electron microprobe analysis do not yield accurate quantitative measurements of alloy composition; only relative variations can be detected.

How do we ensure conservation of solute if $\bar{C}_s$ within a random volume element is greater than or equal to C_0? This is simply a matter of faith. There have been no analytical calculations, or numerical models, reported in the literature which rigorously demonstrate global conservation of solute after duly accounting for ALL important effects, in particular fluid-flow effects. We simply ASSUME solute conservation: i.e., regions in the casting wherein $\bar{C}_s > C_0$ are exactly matched by regions wherein $\bar{C}_s < C_0$. It is easy to demonstrate, with some useful simplifications, that when fluid flow effects are included, $\bar{C}_s$ is equal to C_0 only in the special case when k = 1 [15].

$$\bar{C}_s = C_0[\frac{k}{k'} + (1 - \frac{k}{k'})g_E^{k'}] \tag{2}$$

$$\text{where } k' = 1 - \frac{(1-k)}{(1-\beta)(1+\xi)} \tag{3}$$

ξ = v. $\Delta T/\epsilon$ is the fluid flow parameter, assumed to be constant throughout solidification. v is the fluid flow velocity within the element, ∇T is the thermal gradient and ϵ is the cooling rate. g_E is the volume fraction eutectic in the element. $g_E = f_E$ if β = 0. Equations (2) and (3) are derived in reference 15. For = 0 and β = 0, equations (2) and (3) indicate that $\bar{C}_s$ is always equal to C_0, that there is NO macrosegregation and ONLY microsegregation within the volume element of Figure 7.

---

* The casting may also be a "microcasting" such as a rapidly solidified powder particle or melt spun ribbon [15].
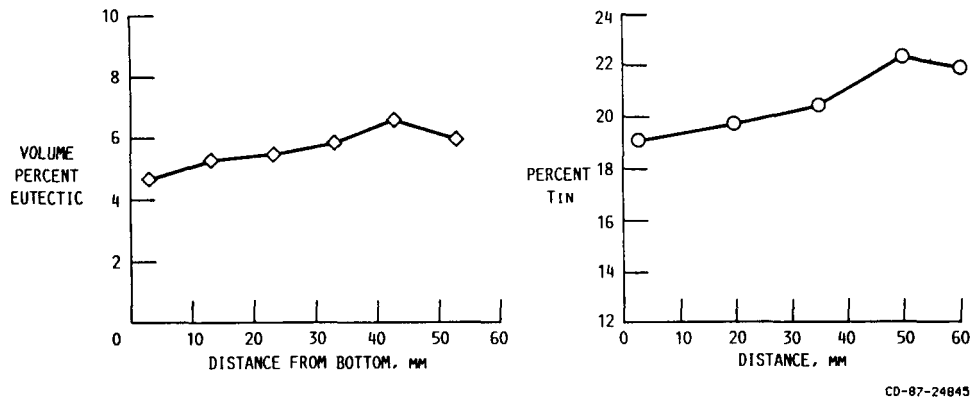
CD-87-24845

Fig. 9 : Comparison of fraction eutectic measurement and tin content
measurements for slow cooled MSFC test. Tin content was obtained
from a coarse beam raster, in a microprobe. The probe averages
the composition across several dendrite and eutectic regions,
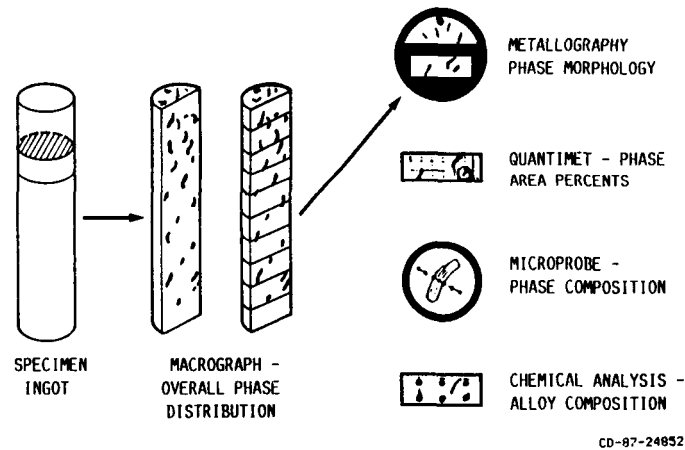such as shown in the quantimet image field micrograph of fig. 11.

CD-87-24852

Fig. 10 : Sequence of analysis of GPF samples after isothermal or non-
isothermal processing.

Thus, fluid flow and shrinkage effects are the underlying cause of macrosegregation in terrestrial solidification processes. Carefully controlled microgravity experiments would help verify the simple analytical calculation presented here. This must of course be coupled with a more rigorous numerical calculation. The crux of the matter quite simply is the evaluation of the spatial and temporal variation of the fluid flow parameter ξ or the "effective" partition ratio, k' as defined by Equation (3). Spatial variations of $\bar{C}_s$ in the final ingot arise,

simply speaking, from the spatial variation of k' during solidification.

To summarize, macro- and microsegregation in an alloy may be quantified by detailed measurements of $\bar{C}_\alpha$, $\bar{C}_s$, f_α, or f_E. Other related

morphological characteristics of interest are i) the tip composition, C_t

or kC_t, i.e., the composition at the centerline of the dendrite in the

finally solidified alloy, ii) the primary and secondary dendrite arm spacings, λ_p and λ_s respectively, iii) the cell or dendrite length, i.e.,

the mushy zone thickness, M. Variation in dendrite arm spacings in the ingot are of particular interest since this suggests variation in the permeability of the dendritic network to fluid flow during solidification. A careful measurement of dendrite arm spacings in 1-g control tests is also important because dendrite arm spacings in reduced gravity experiments have often been reported to be higher than in the 1-g experiments [16-19].

Experimental Results

The isothermally processed samples from the MSFC tests and the samples processed at CWRU have all been subjected to a rigorous regimen of post-mortem metallographic analyses, Figure 10. These include detailed microstructural characterization, viz. primary and secondary dendrite arm spacing measurements using optical metallography techniques, quantimet measurements of area fraction eutectic (two-phase material) in the sample, microprobe measurements to delineate microsegregation across individual dendrites, and a coarse beam raster to arrive at a qualitative measure of macrosegregation. Finally, a more detailed macrosegregation characterization was performed by actual chemical composition measurements of small drillings from various random locations. Such destructive chemical measurements have been kept to a minimum. Indeed, one of our objectives in this program has been to establish that non-destructive techniques such as fraction eutectic measurements with a quantimet offer a very reliable alternative.

The quantimet provides very accurate measurements of the area fractions of the dendrite and eutectic phases at any given location. The accuracy of the quantimet measurements depends on the ability of this instrument to detect various shades of grey. In a carefully prepared sample, the dendrite and eutectic phases etch differently; the dendrite phase often appears much much darker than the eutectic phase. Figure 11 illustrates a typical microstructure, or image field, used in the quantimet measurements. Each image field is a rectangular box approximately 650 microns by 400 microns. Typically about 800 such image field measurements can be obtained in a single transverse cross-section of the sample. The average of these 800 or so quantimet measurements gives the area fraction eutectic at say a given distance from the bottom of the ingot.

10 MM

38 MM

CD-87-24796

10 MM
38 MM FROM BOTTOM

38 MM FROM BOTTOM
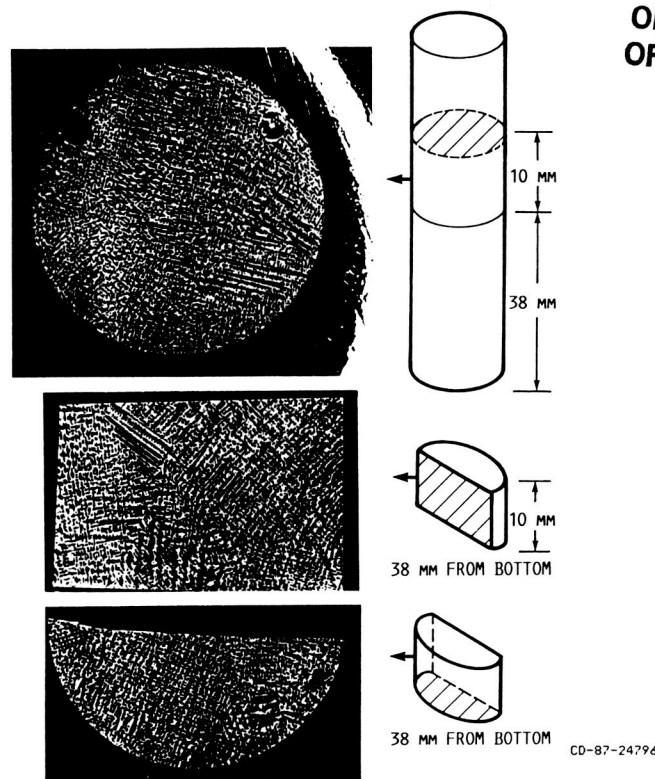
Fig. 11a : Low magnification photomicrographs illustrating dendritic growth
in a partially frozen and quenched sample of Pb-15 wt% Sn alloy.

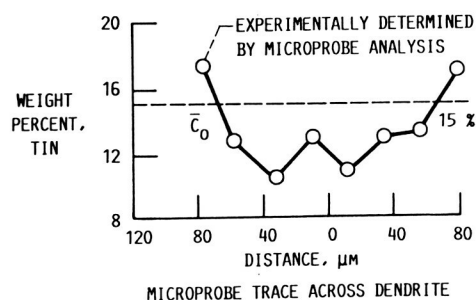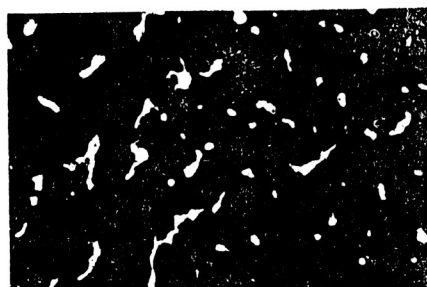TYPICAL QUANTIMET IMAGE
FIELD FOR FRACTION
EUTECTIC MEASUREMENT -
LIGHT AREAS ARE EUTECTIC

HIGHER MAG PICTURE OF EUTECTIC
DENDRITE REGION THICKNESS
~270 μM

EXPERIMENTALLY DETERMINED
BY MICROPROBE ANALYSIS

WEIGHT
PERCENT,
TIN

$\bar{c}_0$

15 %

DISTANCE, μM

MICROPROBE TRACE ACROSS DENDRITE

CD-87-24797

Fig. 11b : Image field for fraction eutectic measurement and a higher magni-
fication picture of dendrite and eutectic regions. Note the sharp
boundary between the dendrite and eutectic regions. Also indicated
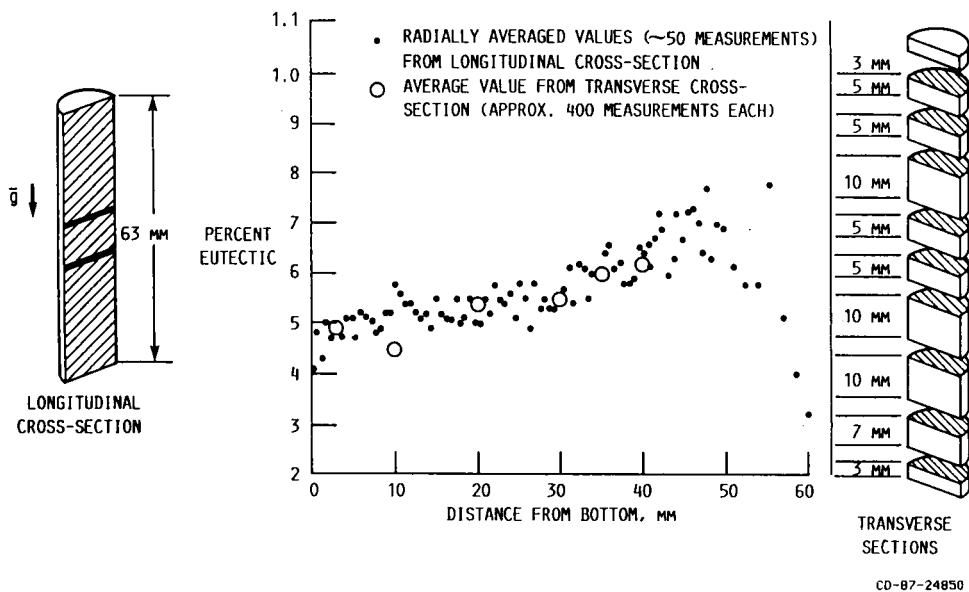is the microsegregation profile across the dendrite region.

Fig. 12 : Fraction eutectic measurements in slow cooled sample, processed
isothermally in the GPF single cavity simulator. Thermal
conditions in this experiment are identical to those to be employed
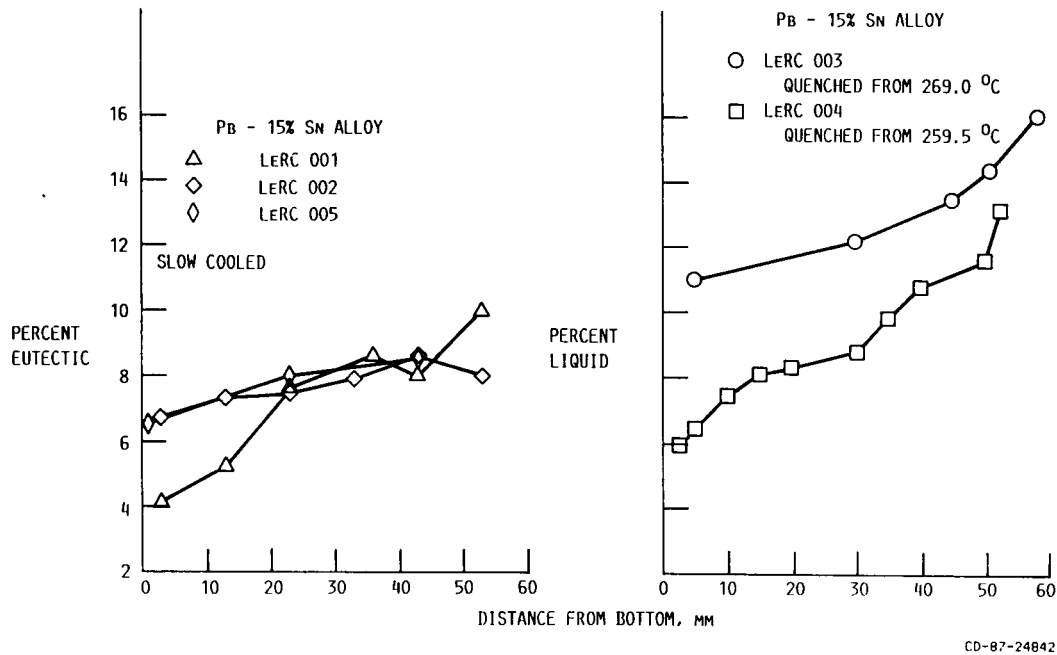in the microgravity experiment.

Fig. 13 : Summary of fraction eutectic and fraction liquid in isothermally
processed samples; MSFC tests, table 1.

(The full circular cross-section yields about 800 or more measurements, the semi-circular sections yield up to 450 measurements, a complete longitudinal cross-section yields over 1250 measurements).

Figure 12 provides an example of our fraction eutectic measurements for one of the MSFC test samples. Each data point here (solid dots) represents an average of about 50 measurements made in a longitudinal cross-section. This thus gives us a radially averaged measurement. The large open circles here are measurements made in a transverse (semi-circular) cross-section. Each one of these open circles now represents an average of about 450 measurements, which accounts for both radial and circumferential variations at that height. Both sets of measurements indicate the same trend: the fraction eutectic increases gradually from the bottom to the top of the ingot. This suggests an enrichment of the remanent liquid with Sn and a gradual floating of the lighter Sn-enriched liquid to the top of the ingot during the unusually long solidification time (640 minutes or about 11 hours) experienced by this slowly cooled ingot. This is also confirmed by the coarse beam microprobe measurements, Figure 12b.

Figure 13 summarizes the results obtained from the various MSFC tests. In some of these tests solidification was interrupted by rapidly quenching the sample prior to complete solidification. In this case the quantimet measurements give the fraction of liquid remaining in the sample at various locations just prior to the initiation of the quench. The quenched liquid has a very fine structure and again etches differently in a carefully prepared sample.

Figure 14 plots the radial segregation pattern at various fixed distances from the ingot bottom; i.e., the variation in fraction eutectic with distance measured from the axis of the ingot. We are simply re-plotting here the measurements taken in the longitudinal cross-section of Figure 12. Each data point in Figure 14 represents the very "local" measurement, at that point. Note that radial variations of fraction eutectic are quite small near the bottom of the ingot, but large radial variations are observed in the top half of the ingot. This radial segregation pattern is somewhat reminiscent of the segregation profiles observed in many earth-growth semi-conductor crystals (PbSnTe, HgCdTe, Ga-doped Ge, for example) wherein the solidification morphology is much more simple [23] - a planar interface as opposed to the intricate dendritic pattern here.

Figure 15 summarizes our secondary dendrite arm spacing measurements. The numbers within the parenthesis represent the number of measurements taken in each of the samples to arrive at the average value reported here. Figure 16 is an example of the composition measurements in the CWRU tests. A more detailed report of the MSFC and CWRU test results is under preparation [20, 21].

Modeling of Segregation Behavior

In this section some preliminary semi-analytical calculations are described which were aimed at pinpointing some of the important elements of a satisfactory theoretical model for segregation behavior. A full numerical simulation, which includes fluid-flow effects, is also being developed to describe more completely the rather complex and interesting radial and longitudinal segregation pattern observed in the isothermally processed samples.
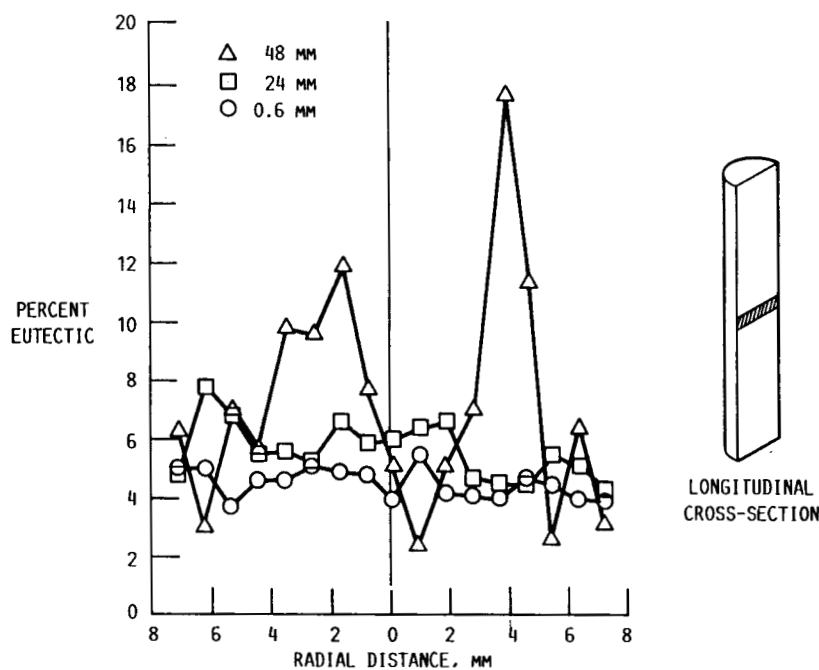
Fig. 14 : Radial segregation pattern in isothermally processed sample.

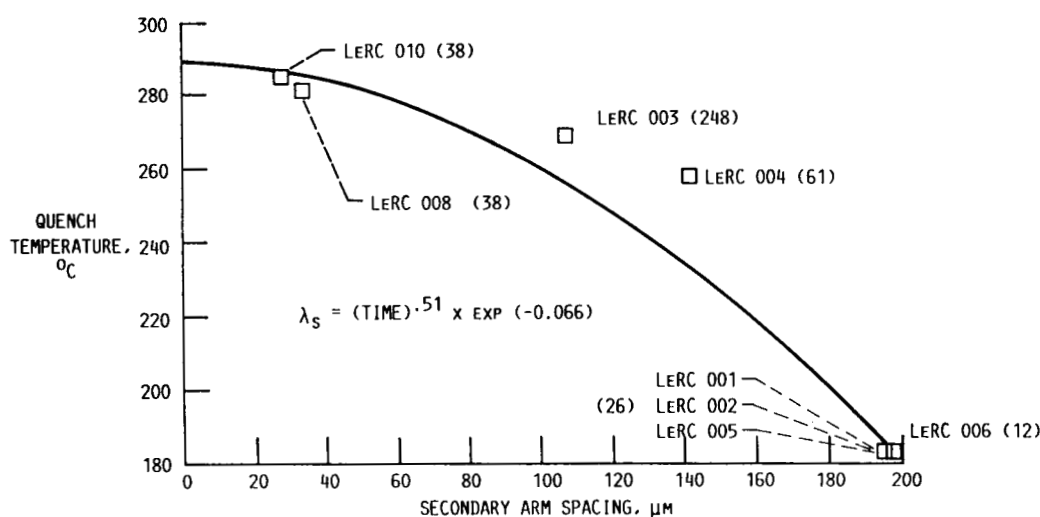$$\lambda_s = (TIME)^{.51} \times EXP (-0.066)$$

Fig. 15 : Summary of secondary dendrite arm spacing measurements in iso-
thermally processed samples. Numbers in parantheses indicate the
number of measurements per sample. Note that the secondary dendrite
spacing is quite fine in samples wherein solidification was interr-
upted at high temperature. These interrupted tests show that in the
completely solidified sample, the spacing increases from about 20
microns at the early stages of solidification to the final value
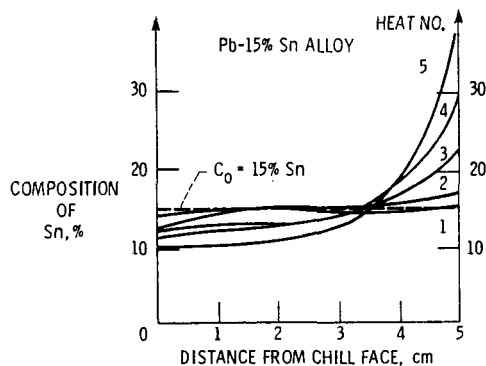of about 200 microns. This phenomenon is called coarsening.

446

Fig. 16 : Summary of composition measurements (using a diffuse microprobe beam as in fig. 9) in the slow cooled samples processed at CWRU.

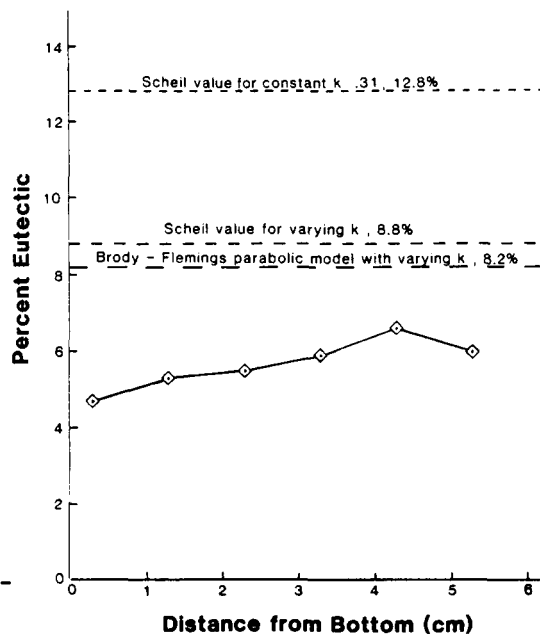
Distance from Bottom (cm)

Fig. 17 : Comparison of fraction eutectic measurements with the predictions of various models for segregation. The models predict the maximum eutectic fraction in a randomly located volume element. Fluid flow is neglected.
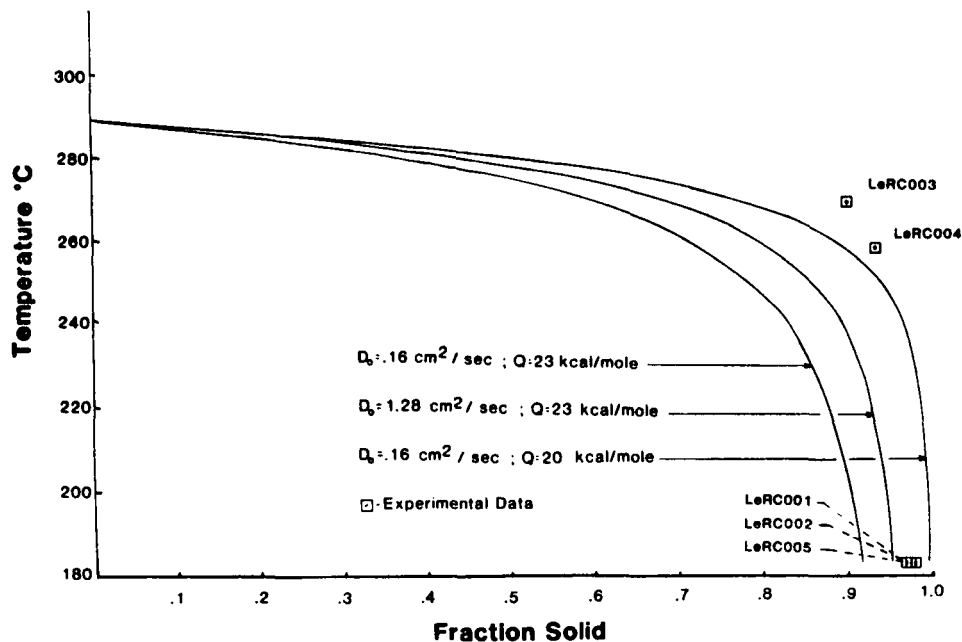

Fraction Solid

Fig. 18 : Theoretical plots of fraction solid versus temperature for various theoretical models. The amount of solid formed at the eutectic temperature is the fraction eutectic predicted in the finally solidified alloy. A high diffusion coefficient of tin in the solid implies tin content in the dendrite and hence smaller amounts of eutectic in the final solid.

447

The analytical calculation is simply aimed at determining the maximum amount of eutectic that would be formed in the sample, within a random volume element such as considered in Figure 7. We completely neglect fluid-flow effects as a first step, i.e., the fluid-flow parameter is taken to be small compared to unity and we set $\beta = 0$. The differential solute balance (see Table 3) may be readily integrated with these approximations if we also assume the partition ratio k to be constant. The integrated result is actually the same as the familiar Scheil equation [22]. However, in this case, the Scheil equation gives the "local" variation in composition within a small volume element, rather than the variation of composition from one end of the ingot to the other, as in semiconductor crystal growth [23, 24]. (In electronic crystal growth applications, the solid morphology is planar and the entire ingot is taken as the volume element in the differential balance; see also Flemings in reference 25. Here the volume element for the differential solute balance is of the order of the dendrite arm spacings). For the Pb-15 wt% Sn alloy with k = 0.31, this yields a fraction eutectic of about 12.8%. This is much higher than the maximum, radially averaged, value determined in these experiments and is represented by the horizontal line in Figure 17.

The partion ratio k is however not a constant and varies from about 0.50 close to the liquidus temperature to about 0.31 close to the eutectic temperature. Allowing for a varying k and performing a numerical integration of the Scheil balance yields a much lower fraction eutectic, 8.8 % compared to 12.8% with constant k.

Next we allowed for some diffusion of the rejected solute into the solid, i.e., we consider a two-sided model for segregation. Two such models were proposed by Brody and Flemings [26] and this was subsequently modified by Clyne and Kurz [27]. "Back-diffusion" or diffusion in the solid is characterized by the dimensionless parameter $\alpha = D_s t_f / \lambda_s^2$, where D_s is the diffusion coefficient of Sn in the solid and t_f is the "local" solidification time. Clyne and Kurz defined another dimensionless parameter α' which is a function of α. A large value of α or α' implies a significant contribution from diffusion in the solid. Diffusion of solute into the solid will increase the average solute content of the dendrite (C_α) and hence reduce the amount of eutectic formed. We again performed a numerical integration of the differential solute balance and allowed for i) varying k with temperature and composition, ii) variation in dendrite arm spacing with during solidification, which we deduced from our interrupted quench tests, Figure 15, iii) variation in diffusion co-efficient temperature. The results of these calculations are shown in Figures 17 and 18. The maximum value of f_E predicted is now only about 8.2% which is much closer to the maximum value (radially averaged) of about 6% in our experiments.

Again, these preliminary semi-analytical calculations only point out the important ingredients of a more complete analysis which must necessarily include fluid-flow effects. Only such a calculation will be able to re-capture the details of both the longitudinal and radial segregation pattern reported here.

Table 3: SUMMARY OF VARIOUS THEORETICAL MODELS FOR SEGREGATION BEHAVIOR IN BINARY ALLOYS

MODEL	Reference Number	Assumptions	Differential Solute Balance	Integrated Solute Redistribution Equation	Comments
Gulliver (1913)	29	• No concentration gradients in liquid (Complete mixing assumption)	$\dfrac{df_L}{f_L} = -\dfrac{dC_L}{C_L(1-k)}$	$C_s^* = kC_0(1-f_s)^{k-1}$ Scheil Equation	• Entire ingot is the volume element for solute balance when applied to predict segregation during semiconductor crystal growth; Model predicts variations from end to end of ingot in this case, ref. 24
Hayes & Chipman (1938)	30	• No diffusion of rejected solute into solid during freezing; one-sided model			
Scheil (1942)	22	• Planar interface			• $\bar{C}_s = C_0$ for all values of k
Brody & Flemings (1966) (BF)	26	• No concentration gradients in liquid; • Some diffusion of rejected solute into solid during freezing; two-sided model; • Linear rate of thickening of dendrite arms; • Same as above, but parabolic rate of thickening of dendrite arms	$\dfrac{df_L}{f_L + \alpha k} = -\dfrac{dC_L}{C_L(1-k)}$ $\dfrac{df_L}{f_L(1 - 2\alpha k) + 2\alpha k} = -\dfrac{dC_L}{C_L(1-k)}$	$C_s^*=kC_0[1- \dfrac{f_s}{1-\alpha k}]^{k-1}$ Linear model; $C_s^* = kC_0 \ X$ $\{1-(1-2\alpha k)f_s\}^{\frac{k-1}{1-2\alpha k}}$	• For $\alpha=0$ or $\alpha'=0$ BF or CK models reduce to Scheil equation, although applied for dendritic growth; • Volume element during dendritic growth has a length equal to λ_p or λ_s, fig. 8, not entire ingot length as when Scheil equation is used for crystal growth (plane front solidification)

Table 3: SUMMARY OF VARIOUS THEORETICAL MODELS FOR SEGREGATION BEHAVIOR IN BINARY ALLOYS (Cont.)

MODEL	Reference Number	Assumptions	Differential Solute Balance	Integrated Solute Redistribution Equation	Comments
Clyne & Kurz (1981)	.27	Same as for Brody & Flemings parabolic model except α is replaced by α'		$\alpha'=\alpha[1-\exp(-\frac{1}{\alpha})]-\frac{1}{2}\exp(-\frac{1}{2\alpha})$	• For both BF and CK models, $\overline{C}_s = C_o$ only for special values of α(or α'). These models thus violate conservation of solute within the volume element. Note, solute cannot enter or leave volume element by any means, see FN model below.
Flemings and Nereo (1967) (FN)	33	• No concentration gradients in liquid (although there is a temperature gradient across volume element, fig. 7)			• $\overline{C}_s \neq C_o$ in general. $\overline{C}_s = C_o$ for k'=1 i.e. k=1 and/or $\beta=0,\xi=0$
Mehrabian, Keane and Flemings (1970) (MKF)	2	• No diffusion of rejected solute into solid; one-sided model • Solute can enter or leave volume element because of fluid flow • Fluid flow is mainly due to shrinkage for FN	$\dfrac{\partial g_L}{g_L} = - \dfrac{\partial C_L}{C_L(1-k')}$ $k'=1-\dfrac{(1-k)}{(1-\beta)(1+\xi)}$	• $C_s^* = k'C_o(1-f_s)^{k'-1}$ if ξ,β,k constant • Only numerical integration possible when $\xi\neq0$, i.e. $\overline{V}\neq0$	• Since solute can enter or leave volume element because of fluid flow, it is assumed that there is global conservation of solute

450

Table 3: SUMMARY OF VARIOUS THEORETICAL MODELS FOR SEGREGATION BEHAVIOR IN BINARY ALLOYS (Cont.)

MODEL	Reference Number	Assumptions	Differential Solute Balance	Integrated Solute Redistribution Equation	Comments
		• MKF model includes both shrinkage and gravity-induced flow. Darcy's law used to model flow.	$\xi = \bar{V} \cdot \nabla T/\epsilon = \dfrac{\bar{V} \cdot \nabla C_L}{\partial C_L/\partial t}$		
Poirier (1983)	5	• Same as for FN and MKF except that there is a concentration gradient in the liquid • Unidirectional solidification only considered	$\dfrac{\partial g_L}{g_L + \left(\dfrac{\beta_E g_E}{1-\alpha}\right)} = \dfrac{(1-\alpha)\partial C_L}{\dfrac{\alpha \rho_L}{m_\rho} - (1-k) C_L}$ $\beta_E = \dfrac{\rho_{sE} - \rho_s}{\rho_s}$ $\alpha = \dfrac{D_L G_L^2}{\rho_s \epsilon \tau}\left(\dfrac{m_\rho}{m_L}\right)$ $\tau = D_L/D_{eff} =$ tortuosity $m_\rho = \partial \rho_L/\partial T$	• Only numerical integration possible in general	• $\bar{C}_s \neq C_o$ in general as for FN or MKF. • Global conservation of solute assumed.

Table 3: SUMMARY OF VARIOUS THEORETICAL MODELS FOR SEGREGATION BEHAVIOR IN BINARY ALLOYS (Cont.)

MODEL	Reference Number	Assumptions	Differential Solute Balance	Integrated Solute Redistribution Equation	Comments
Flemings (1964) Bower, Brody and Flemings (1966) (BBF)	31 32	• Solute can enter or leave volume element but only because of diffusion. There is a concentration gradient in the liquid, in a direction perpendicular to the growth direction of array • There is no concentration gradient lateral to growth direction of array, i.e. liquid within volume element, fig. 8, is uniform in composition. • Concentration gradient in interdendritic liquid is constant. Exponential decay in bulk liquid ahead of tips	$$\frac{df_L}{f_L} =$$ $$\frac{dC_L}{-C_L(1-k)-s\Delta C_0}$$ • $s=\dfrac{ak}{k-1}$ $a=\dfrac{D_L G_L}{m_L R C_0}$ • $s = -\dfrac{D_L G_{cI}}{R\Delta C_0}$ • $G_{cI} = G_L/m_L$	$$C_s^* =$$ $$C_0[s+k(1-s)f_L^{k-1}]$$ Note for s→0, i.e. no concentration gradient in interdendritic liquid, model reduces to Scheil equation	• Assumption of exponential decay ahead of tips can be relaxed • It may be shown that solute conservation is obeyed, i.e. $\bar{C}_s = C_0$ for all values of s $\bar{C}_\alpha = C_0[s(1-f_L) +$ $(1-s)(1-f_L^k)]$ For $f_L \to 0$ $\bar{C}_\alpha \to C_0$ i.e. $\bar{C}_s \to C_0$ • First solid to form in volume element has composition $kC_t > kC_0$, i.e. dendrite tips are undercooled
Solari & Biloni (1980)	34	This model attempts to combine the BBF model and the BF model. The dendrite tip composition is calculated from the Burden & Hunt analysis rather than the BBF analysis.			Solute conservation within the volume element is again violated.

452

Table 3: SUMMARY OF VARIOUS THEORETICAL MODELS FOR SEGREGATION BEHAVIOR IN BINARY ALLOYS (Cont.)

MODELS	Reference Number	Assumptions	Differential Solute Balance	Integrated Solute Redistribution Equation	Comments
Laxmanan (1985/87)	9-11, 15, 28	• Same as for BBF model except that isoconcentrates are non-planar in the immediate vicinity of tips • Multi-dimensional diffusion near tips treated approximately by two models. • $\lambda = \phi/2p$ Diffusion field in vicinity of tips is given by Ivantxov solution in the ideal case when $G_L=0$, i.e. dendrite surface is isothermal • $\lambda= 1/16$ Diffusion field in vicinity of tips given by a generalization of the Zener treatment, in the ideal case of $G_L = 0$, instead of Ivantsov.	$\dfrac{df_L}{f_L} = \dfrac{dC_L}{C_L(1-k)-q\Delta C_0}$ • $s = \dfrac{ak}{k-1}$ $a = \dfrac{D_L G_L}{m_L R C_0}$ • $G_{cI} \neq G_L/m_L$ • $\dfrac{\Delta C}{\Delta C_0} = \dfrac{2p\lambda k}{b}[1+\dfrac{s}{k}\tilde{N}_g(p)]$ • $\tilde{N}_g(p) = (1-2p\lambda)/2p\lambda$ • $b = 1-2p\lambda(1-k)$	• $C_s^* = C_0\{q+k(1-q)f_L^{k-1}\}$ • $\bar{C}_\alpha = C_0[q(1-f_L)+ (1-q)(1-f_L^k)]$ Note for $f_L\to0$, $\bar{C}_\alpha\to C_0$ for all values of q • For $q\to0$, i.e. for $G_{cI}\to0$ model reduces to Scheil equation	• Model satisfies solute conservation since $\bar{C}_\alpha \to C_0$ for $f_L \to 0$ i.e. $\bar{C}_s \to C_0$ for $f_L\to0$ • When $G_{cI} = G_L/m_L$, q=s, i.e. model reduces to BBF • $q = \Delta C/\Delta C_0$ is in general greater than s. • Unknown Peclet number p, i.e. tip radius is determined either from minimum tip undercooling assumption or from the marginal stability hypothesis, ref. 9. • First solid to form in volume element has composition $kC_t > kC_0$, i.e. $\Delta T > 0$.

453

Future Plans: Summary and Conclusions

1.   A rather intricate longitudinal and radial segregation pattern has been observed in the isothermally processed samples. These results suggest significant gravity-driven fluid-flow effects. The microgravity experiment should indicate a much less pronounced variation of fraction eutectic. A numerical simulation of the 1-g data and the anticipated microgravity results is being planned.

2.   The isothermally processed MSFC samples have been subjected to a rigorous regimen of detailed post-mortem metallographic analyses. Several thousand measurements per sample have already been performed (more are under way), and several important morphological details have been measured. In particular the detailed characterization of the primary and dendrite arm spacings in the samples is a pre-requisite to satisfactory numerical modeling of fluid-flow effects. These measurements were also carried out in anticipation of reportedly larger values of the dendrite arm spacings in other reduced gravity experiments, particularly those performed in the KC-135 flights, compared to the corresponding 1-g spacings.

3.   Thermal conditions to be employed for the microgravity experiment have been shown to be reproducible in several repeat tests (12 to date). The majority of these tests were conducted with the axis of the sample oriented in the direction of the gravity vector. The single-cavity simulator of the GPF at MSFC is mounted on trunions and allows for many different orientations. It would be extremely desirable to perform additional tests in the single-cavity simulator with at least 3 or 4 different angular orientations with respect to gravity vector; 30, 45, 90, 180. These tests were intentionally deferred thus far since our goal was to first develop a satisfactory engineering design of the spring-loaded specimen cartridge. The additional tests mentioned here would indicate the role of gravitational convection in establishing the (very reproducible) thermal profiles obtained thus far in the MSFC experiments. The final programming of the GPF for the microgravity experiment must take into account the outcome of these additional tests. (The springs loaded plunger has been included to eliminate the complicating effects of Marangoni convection associated with a free liquid/gas interface).

4.   Ground-based results already in hand (CWRU tests) indicate a rich variety of experiments that could be gainfully performed in follow-up shuttle experiments. These follow-up experiments should be performed without the isothermal constraints of the first experiment, in the GPF, or other suitably modified shuttle hardware: for example, the Automatic Advanced Directional Solidification Furnace (AADSF) with a stationary sample of appropriate aspect ratio, or even the Isothermal Dendrite Growth Apparatus (IDGA). Both pieces of hardware are currently under development.

5.   Finally, the currently approved and other proposed shuttle experiments in this series have been planned in a manner that would allow both a more fundamental understanding of the role of gravity during solidification as well as yield information of great value from an engineering standpoint.

NOMENCLATURE

R — Dendrite tip growth rate

T_L — Liquidus temperature, alloy melt

T_s — Solidus temperature

T_t — Dendrite tip temperature

ΔT — Tip "undercooling", $(T_L - T_t)$

C_0 — Initial alloy composition

C_t — Liquid composition at tip

C_t^0 — Liquid composition at tip, isothermal case

ΔC — Solute buildup at tip, $(C_t - C_0)$

G_c — Concentration gradient at tip, non-isothermal case

G_i — Interdendritic thermal gradient, in liquid

G_L — Thermal gradient in liquid, at tip

G_{cI} — Concentration gradient in inter-dendritic liquid

m_L — Slope of equilibrium liquidus line

k — Partition ratio, assumed constant. May or may not be equilibrium value.

ΔC_0 — Solute buildup for plane front, steady state: $C_0(1-k)/k$

ΔT_0 — Undercooling at planar interface, steady-state, $(T_L - T_s)$ = $-m_L \Delta C_0$

D_L — Diffusivity of solute in liquid

Ω — Supersaturation at tip, non-isothermal case, $\Delta C/C_t(1-k)$

Ω^0 — Supersaturation at tip, isothermal case, $\Delta_D^0/C_t^0 \ (1-k)$ = $2p\lambda$ in general

$\Delta C/\Delta C_0$ — Dimensionless solute buildup at tip

p — Solute Peclet number, $Rr_t/2D_L$

r_t — Tip radius of dendrite

ϕ — Ivantsov function, solute case, $pe^p E_1(p)$

λ — Solutal lambda, Zener number, $\Omega^0/2p$

$\lambda = \phi 2p$, "Point" effect from Ivantsov

$\lambda = 1/16$, "Point" effect from generalized Zener

s — Chalmers number, $D_L G_L/R\Delta T_0$; $D_L G_i/R\Delta T_0$

q — Dimensionless parameter $- D_L G_{cI}/R\Delta C_0$

f_E, g_E — Fraction eutectic or two phase

ξ — Fluid Flow parameter

k' — Effective partition ratio

$\bar{C}_s$ — Average composition of solid when $g_s = 1$

$\bar{C}_\alpha$ — Average composition of dendrite

C_E — Eutectic composition

λ_p — Primary dendrite arm spacing

λ_s — Secondary dendrite arm spacing

M_* — Mushy zone thickness

C_s^* — Solid composition at interface

C_L^* — Liquid composition, at interface

ρ_{sE} — Density of two-phase, eutectic solid

β, β_E — Fractional density change

α, α' — Dimensionless groups, determine diffusion in solid.

455

References

1. M.C.Flemings, Scand. J. Metallurgy, 5, 1-15 (1976).
2. R.Mehrabian, M.Keane and M.C.Flemings, Met.Trans., 1, 1209, 1970.
3. S.M.Copley, A.F.Giamei, S.M.Johnson and M.F.Hornbecker, Met.Trans., 1, 2193 (1970).
4. A.Sample and A.Hellawell, Met.Trans B, 13B, 495 (1982).
5. D.Poirier, in U.S.-Japan Co-operative Science Program Seminar on Solidification Processing, June 26-29, 1983, Dedham, Mass. Proc.Eds. G.Ohira and M.C.Flemings.
6. T.L.Bergman and A.Ungan, Int.J.Heat & Mass Transfer, 11, 1695 (1986), also, T.L.Bergman, F.P.Incorpera and R.Visankta, J.of Heat Transfer, Trans. ASME, 108, 206 (1986).
7. V.Laxmanan, Science Requirements Document for STS-experiement on "Isothermal Solidification in a Binary Alloy Melt," October 1984.
8. H.Esaka and W.Kurz, J.Cryst.Growth, 72, 578 (1985).
9. V.Laxmanan, J.Cryst. Growth 75, 573 (1986).
10. V.Laxmanan, J.Cryst. Growth, 77 (1987) in press.
11. V.Laxmanan, Acta Met 33, 1023, 1037, 1475 (1985).
12. R.Trivedi, J.Cryst.Growth, 49, 219 (1980).
13. M.C.Flemings, in Solidification Processing, McGraw Hill pp 31-36, (1974).
14. M.C.Flemings, in ref.13, pp 110-112.
15. V.Laxmanan, in Processing and Properties of Structural Metals via Rapid Solidification Processing, to be published by ASM, Metals Park, Ohio. Eds. F.H.Froes and D.J.Savage (in press).
16. M.H.McCay, J.E.Lee and P.A.Curreri, Met.Trans A, 17A, 2301 (1986).
17. M.H.Johnston, P.A.Curreri, R.A.Parr and W.S.Alter, Met.Trans A , 16A, 1683 (1985).
18. R.A.Parr and M.H.Johnston, Met.Trans A, 9A, 1825 (1978).
19. M.H.Johnston and C.S.Griner, Met.Trans A, 8A, 77 (1977).
20. L.Wang, "Gravitational Macrosegregation in Pb-Sn Alloys", M.S. Thesis, Dept. of Metallurgy and Materials Science, Case Western Reserve University, 1985.
21. A.Studer, "Macrosegregation in Isothermally Processed Pb-Sn Alloys", M.S. Thesis, Dept. Of Metallurgy & Materials Science, Case Western Reserve University, thesis in progress.
22. E. Scheil, Z.Metallkunde, 34, 70 (1942).
23. S.L.Lehoczky and F.R.Szofran in Materials Processing in the Reduced Gravity Environment, MRS Symp Proc. Ed.G.E.Rindone, p 409 (1982).
24. R.K.Crouch, A.L.Fripp, W.J.Debnam, I.O.Clark and F.M.Carlson, in ref. 23, p 611.
25. M.C.Flemings, in ref. 13, pp 77-83, 141-146, (1974).
26. H.D.Brody and M.C.Flemings, Trans. AIME, 236, 615 (1966).
27. T.W.Clyne and W.Kurz, Met.Trans A, 12A, 965 (1981).

28. V.Laxmanan, "Analysis of Microsegregation During Cellular and Dendritic Solidification", in preparation.
29. G.H.Gulliver, J.Inst.Metals, 9, 120-157 (1913).
30. A.Hayes and J.Chipman, Trans AIME, Proc. of Detroit Meeting, Oct. 1938, p 85.
31. M.C.Flemings, Trans AFS, 72, 353, (1964).
32. T.F.Bower, H.D.Brody and M.C.Flemings, Trans. AIME, 236, 624 (1966).
33. M.C. Flemings and G.E. Nereo, Trans AIME 239(1967) 1449, 242 (1968) 41,50.
34. M.Solari and H.Biloni, J.Cryst. Growth, 49, 451, (1980).